Wide-Field-of-View Modulating Retro-Reflector System Based on a Telecentric Lens for High-Speed Free-Space Optical Communication

Jiahan Tian, Tingbiao Guo, Nan He, Ji Du, Qiangsheng Huang, Xiaojian Hong, Chao Fei, Yuan Wang, Tianyi Zhang, Junping Zhang, and Sailing He, *Fellow, IEEE*

***Abstract*—Modulating retro-reflector (MRR) free-space optical (FSO) communication technology presents a bright future for realizing the small size, weight, and power (SWaP) design of one end of the optical link, facilitating the further application of the FSO communication to the small platforms. However, the limited field-of-view (FOV) of MRR impedes its wide employment. In this article, a novel wide-FOV MRR using an image space telecentric lens is proposed and a bidirectional FSO communication system is experimentally demonstrated using this MRR with a single light source. The performance of the telecentric lens between the transceiver and terminal is assessed by simulation and also validated by experimental results, with a coupling loss less than 9.1 dB within a FOV of 110°. Both 10-Gbit/s on-off keying (OOK) downstream and upstream signals for free space communication at different incident angles are successfully realized using this designed wide-FOV MRR. The experimental results validate the proposed MRR has a FOV of up to 110° where the measured bit error rate (BER) is lower than 3.8×10^{-3} for both downstream and upstream signals. To the best of our knowledge, this is the largest FOV ever reported for MRRs in high-speed bidirectional FSO communication systems.**

Manuscript received 10 June 2023; revised 31 July 2023; accepted 12 August 2023. Date of publication 15 August 2023; date of current version 30 August 2023. This work was supported in part by the National Natural Science Foundation of China under Grants 62105284, 62101486, and 62001415, in part by the Natural Science Foundation of Zhejiang Province under Grant LQ21F050013, in part by the Ningbo Science and Technology Project under Grants 2018B10093, 2020G012, and 2021Z029, and in part by the Natural Science Foundation of Ningbo under Grant 2023J283. *(Jiahan Tian, Tingbiao Guo, and Nan He contributed equally to this work.) (Corresponding authors: Tingbiao Guo; Junping Zhang; Sailing He.)*

Jiahan Tian, Tingbiao Guo, Nan He, Ji Du, Xiaojian Hong, Chao Fei, Yuan Wang, and Tianyi Zhang are with the State Key Laboratory of Modern Optical Instrumentation, Centre for Optical and Electromagnetic Research, National Engineering Research Center for Optical Instruments, College of Optical Science and Engineering, Zhejiang University, Hangzhou 310058, China (e-mail: tbguo@zju.edu.cn).

Qiangsheng Huang is with the State Key Laboratory of Modern Optical Instrumentation, Centre for Optical and Electromagnetic Research, National Engineering Research Center for Optical Instruments, College of Optical Science and Engineering, Zhejiang University, Hangzhou 310058, China, and also with the Shanghai Institute for Advanced Study, Zhejiang University, Shanghai 200135, China.

Junping Zhang is with the Huawei Technologies Company, Ltd, Shenzhen 518129, China (e-mail: junping.zhang@huawei.com).

Sailing He is with the State Key Laboratory of Modern Optical Instrumentation, Centre for Optical and Electromagnetic Research, National Engineering Research Center for Optical Instruments, College of Optical Science and Engineering, Zhejiang University, Hangzhou 310058, China, and also with the Department of Electromagnetic Engineering, School of Electrical Engineering, Royal Institute of Technology, SE-100 44 Stockholm, Sweden (e-mail: sailing@zju.edu.cn).

Digital Object Identifier 10.1109/JPHOT.2023.3305512

***Index Terms*—Free-space optical communication, image space telecentric lens, modulating retro-reflector, wide field-of-view.**

I. Introduction

In RECENT years, with the further application of 5G technology, artificial intelligence, big data, and other related technologies, the development trend of the Internet of Things (IoT) makes the communication traffic surge, which puts forward higher requirements for the performance of communication systems [1], [2]. Traditional radio-frequency (RF) communication is approaching to its limit due to limited transmission data rate and spectrum congestion. In contrast, free-space optical (FSO) communications, featuring the benefits of high security, strong anti-jamming ability, high bandwidth, long transmission distance, abundantly available spectrum, and high bit rate that can be stretched up to gigabits and even terabits, are promising supplementary techniques for the implementation of future high-speed wireless communications [3], [4], [5], [6], [7]. However, line-of-sight (LoS) is needed while establishing FSO communication link, which requires an acquisition tracking pointing (ATP) system with massive size, weight, and power (SWaP) in both transceiver and terminal [8], [9], [10]. At present, modulating retro-reflector (MRR) is expected to be used in mobile terminals, which can eliminate the light source and ATP system in the terminal [11], [12], thus reducing SWaP, providing a feasible scheme for the FSO system to be widely used between base stations (e.g., ground platforms) and mobile devices (e.g., aircraft and satellites), where strict requirements on volume, load, and power consumption exists [13], [14], [15].

For the present MRR systems, researchers commonly use corner cubes [16], [17], [18], [19], cat's eyes [12], [14], [20], [21], [22], [23], [24], [25], [26] to retro-reflect optical signals, combined with ferroelectric liquid crystal (FLC) modulators [16], microelectromechanical systems (MEMS) modulators [17], multiple quantum well (MQW) modulators [12], [20], [21], [24] and acousto-optic modulators (AOM) [23], to achieve modulating retro-reflection. For corner cube retro-reflection techniques, Swenson et al. experimentally demonstrated data rates of 1.2 kbit/s for downstream and 20 kbit/s for upstream FSO communication with the FOV of 45° base on FLC modulator [16]. In 2010, Mahon et al. utilized MEMS modulator to realize 8 m/100 kbit/s data rate for upstream FSO transmission [17]. And for

TABLE I
COMPARISON OF MRR SYSTEMS IN THE LITERATURES

Year	Ref.	Light source wavelength (nm)	Rx optics	Modulator	Modulation scheme	Distance (m)	Downstream data rate	Upstream data rate (MRR modulation rate)	FOV(°)
2001	[12]	976	Cat's eye	[a]MQW	OOK	35	910 kbit/s	1.2 Mbit/s	20
2002	[23]	780	Cat's eye	[b]AOM	OOK	-	-	1 Mbit/s	-
2003	[20]	-	Cat's eye	[a]MQW	OOK	-	-	50 Mbit/s	30
2004	[25]	1550	Cat's eye	[c]ARM	OOK	-	-	2.5 Gbit/s	0.0004
2007	[21]	1550	Cat's eye	[a]MQW	OOK	320	-	1 Mbit/s	10
2010	[17]	400-500	Corner cube	[d]MEMS	OOK	8	-	100 kbit/s	-
2017	[24]	1550	Cat's eye	[a]MQW	OOK	200	-	200 Mbit/s	2.8
2017	[26]	1550	Cat's eye	[e]RSOA	[g]DPSK for downlink; OOK for uplink	0.5	10 Gbit/s	1.25 Gbit/s	34.9
2021	[14]	1561	Cat's eye	[a]MQW	OOK	560	-	500 Mbit/s	6.4
2023	**This work**	1550	Telecentric lens (cat's eye)	[f]MZM	OOK	3	**10 Gbit/s**	**10 Gbit/s**	**110**

[a]MQW represents multiple quantum well modulator; [b]AOM represents acousto-optic modulator; [c]ARM represents amplified retro-modulator; [d]MEMS represents microelectromechanical system; [e]RSOA represents reflective semiconductor optical amplifier; [f]MZM represents Mach-Zehnder modulator; [g]DPSK represents differential phase shift keying.

cat's eyes retro-reflection techniques, in 2002, the AOM-based MRR reached 1 Mbit/s upstream data rate [23]. Also they are frequently combined with MQW modulators in MRR. In 2001, the bidirectional communication with the downstream data rate of 910 kbit/s and upstream data rate of 1.2 Mbit/s at a distance of 35 m was reported, where the MRR also accomplished the FOV of 20° [12]. In 2003, Rabinovich et al. raised the upstream data rate to 50 Mbit/s and FOV to 30° with this combination design [20]. In 2007, 320 m FSO communication with the upstream data rate of 1 Mbit/s and the FOV of 10° was conducted [21]. In 2017, Quintana et al. embedded MQW modulator in an asymmetric Fabry–Perot cavity, realizing the FOV of 2.8° and upstream data rate of 200 Mbit/s at the distance of 200 m [24]. And in 2021, Quintana et al. carried out a MRR design with the FOV of 6.4° and upstream data rate of 500 Mbit/s, and also established a FSO communication link between a ground station and an unmanned aerial vehicle with the distance of 560 m [14]. However, the existing MRR structure is facing issues like limited field-of-view (FOV), high energy attenuation, and low modulation rate, which hinders its wide employment. More recently, a novel structure combining a cat's eye retro-reflector with a single-mode fiber (SMF) was proposed in [25], [26]. By coupling the optical signal into the SMF, mature high-speed modulators such as Mach-Zehnder modulator (MZM) can be adopted to greatly improve the data rate and it is possible for monolithic integration of all components of the terminal on circuits, hence greatly reducing the SWaP. In 2004, Shay et al. introduced the amplified retro-modulator (ARM) as MRR design which operates at a data rate of 2.5 Gbit/s with the FOV of 0.0004° [25]. In 2017, Wang et al. proposed a MRR employing a reflective semiconductor optical amplifier (RSOA) achieving the downstream data rate of 10 Gbit/s, upstream data rate of 1.25 Gbit/s, and FOV of 34.9° at the distance of 0.5 m. Nonetheless, the FOV of this configuration in reported works is restricted only within 35 degrees. Table I summarizes the recent research progress of MRR in terms of transmission distance, downstream data rate, upstream data rate (i.e., the MRR modulation rate), and FOV.

To further improve the figure of merit of the MRR systems, in this article, we propose a wide-FOV MRR based on a customized image space telecentric lens and experimentally demonstrate a bidirectional high-speed FSO system. The telecentric lens with a large FOV and high coupling efficiency, ensuring the coaxial propagation path of the incoming beam and the outgoing beam emitted from SMF, can be effectively employed in the MRR structure. For both downstream and upstream optical signals, the maximum coupling loss of the MRR is simulated down to 5.6 dB between −50° and +50°, 6.9 dB between −60° and +60°, 12.1 dB between −65° and +65°, and experimentally measured down to 7 dB between −50° and +50°, 9.1 dB between −55° and +55, and 16.5 dB between −60° and +60°. Thanks to the MRR system, only a single laser source (at the transceiver) is used in the bidirectional FSO system. The upstream signal is modulated on the reflected optical carrier at the terminal. Eye diagrams and bit error rates (BERs) are measured for both downstream and upstream signals within the whole FOV, confirming the validation of the presented MRR system. The experimental results show that the proposed MRR system supports 10-Gbit/s downstream on-off keying (OOK) signals with FOV of up to 120° and 10-Gbit/s upstream OOK signals with FOV of up to 110°, which to the best of our knowledge, is the largest FOV in MRR system for high-speed FSO communication.

II. PRINCIPLES

A. The Design of the Rx Optics

For FSO systems, a wide-FOV MRR in mobile terminals can mitigate the difficulty of coupling alignment and eliminate the bulky tracking system, leading to terminal miniaturization. This requires that the Rx optics have a large FOV and numerical aperture (NA) matching SMFs to ensure the entirely coaxial propagation path and high coupling efficiency of both incident and retro-reflected beams.

Fig. 1(a)–(d) shows a schematic of the beam path for a MRR with different Rx optics configurations. The incident beam emitted from SMF (point A(B)) of the transceiver becomes parallel after passing through the collimator, incident onto the Rx optics, then converges to point A'(B') on the focal plane of Rx optics, whose position depends on the incident angle. By

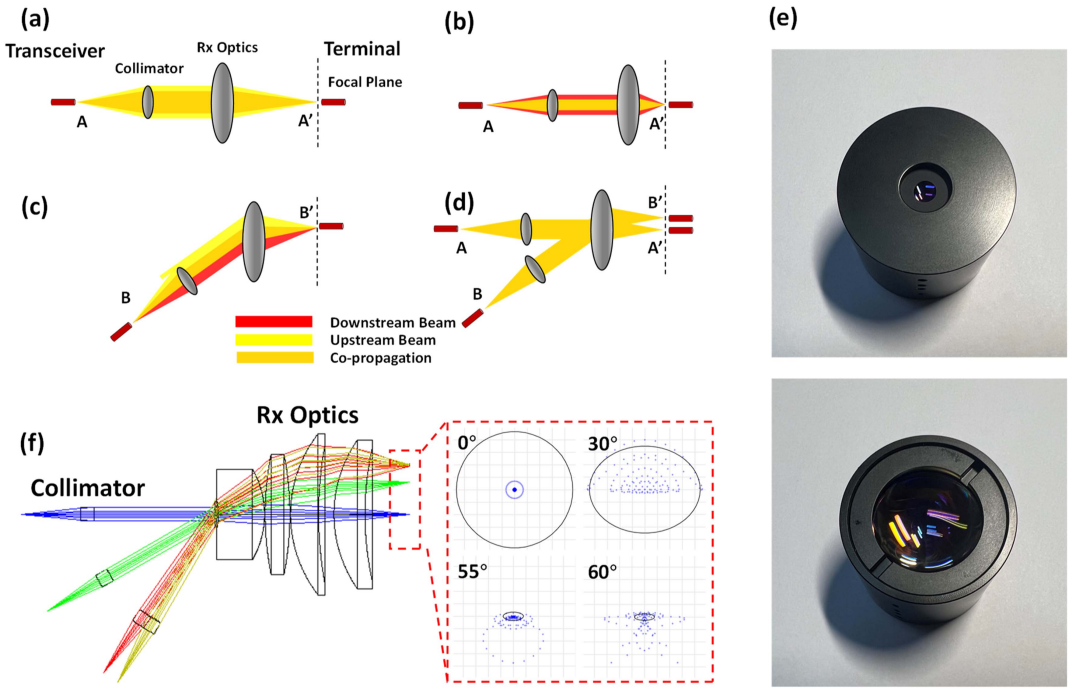

Fig. 1. Optical signal propagation diagram in (a) conventional Rx lens with a smaller NA; (b) conventional Rx lens with a larger NA; (c) conventional Rx lens with matched NA; (d) image space telecentric lens with matched NA; (e) the picture of the fabricated image space telecentric lens; (f) the ray tracing of incident beams and corresponding spot diagrams on the image surface at incident angles of 0°, 30°, 55°, and 60°.

moving the end-face of the SMF by a translation stage to the focal point A'(B'), the incident beam is finally coupled into the SMF of the terminal. Generally, fiber arrays are always used to collect different incident beams on the focal plane, where SMFs are evenly and vertically distributed on the focal plane. They could shorten the lateral distance that the translation stage needs to move while coupling the incident beam into SMF. The retro-reflected beam will propagate from point A'(B') and be coupled into point A(B). The ratio of the overlap between them roughly represents the coupling efficiency of the MRR system. In Fig. 1(a), we show a conventional lens as Rx optics with a smaller NA compared to the SMF. In this scheme, incident beams can be coupled into the SMF with high efficiency, while part of retro-reflected light will be lost. On the contrary, for Rx optics with a larger NA as shown in Fig. 1(b), some of the incident light will be lost while retro-reflected beams can be coupled into the transceiver with high efficiency. These results illustrate that the NA of Rx optics ought to match well with the SMFs for a high-efficient MRR system in the reversible propagation path.

As for the conventional lens with matching NA shown in Fig. 1(c), the propagation path of the incident beam emitted from the axis of Rx optics totally matches the retro-reflected one. However, the propagation path of the beam emitted from the point B off the axis of Rx optics does not match the retro-reflected one since the chief ray of the retro-reflected light from a fiber tip is always parallel to the main axis of the Rx optics, leading to low efficiency. Fig. 1(d) shows that for the image space telecentric lens with matching NA, the co-propagation path for both the on-axis and off-axis light completely matches well, so high coupling efficiency can be achieved.

Therefore, to achieve retro-reflection with high efficiency, the chief ray of both incident and retro-reflected beams ought to coincide and the NA of the Rx/Tx optics is supposed to match the one of SMF. To meet this requirement, we choose an image space telecentric lens with NA matching to SMFs as Rx optics. The lens has a back focal length of 7.55 mm and an entrance pupil diameter of 2 mm (Fig. 1(e)). The coupling efficiency of the Rx optics is simulated by the ray tracing software in this article. The lens system efficiency (S) is first calculated as the sum of the energy collected by the entrance pupil which passes through the optical system, accounting for both the vignetting and transmission of the optics, divided by the sum of all the energy which radiates from a source fiber:

$$S = \left[\frac{\int\int t(x,y)F_S(x,y)\mathrm{d}x\mathrm{d}y}{\int\int F_S(x,y)\mathrm{d}x\mathrm{d}y}\right]^2 \tag{1}$$

where $F_s(x,y)$ is the source fiber amplitude function and the integral in the numerator is only done over the entrance pupil of the optical system, and $t(x,y)$ is the amplitude transmission function of the optics. The transmission is affected by bulk absorption and optical coatings. If the source fiber is ignored, then the integral in the denominator is only done over the entrance pupil, and the $F_s(x,y)$ function is determined by the system apodization.

Aberrations in the optical system introduce phase errors which will affect the coupling into the fiber. Maximum coupling efficiency is achieved when the mode of the wavefront converging towards the receiving fiber perfectly matches the mode of the fiber in both amplitude and phase at all points in the wavefront.

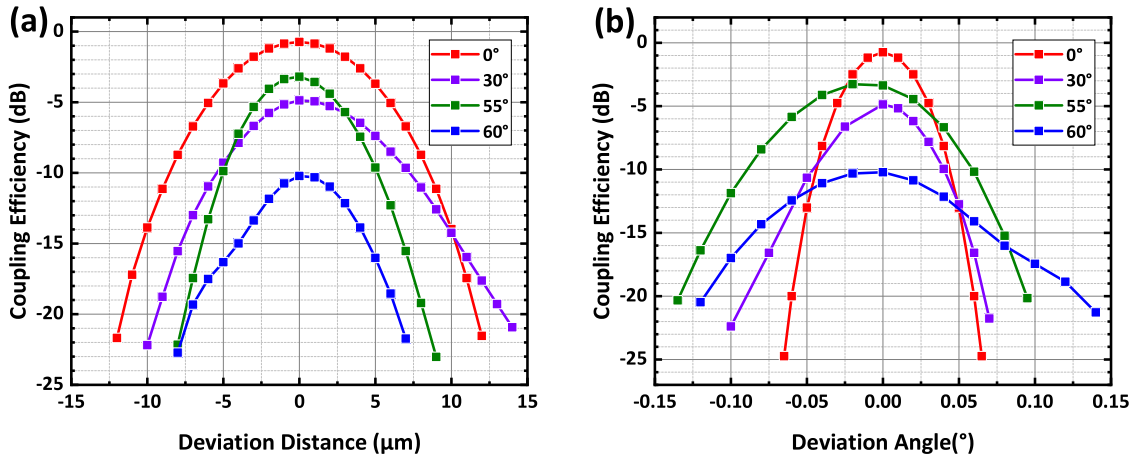

Fig. 2. The coupling efficiency of the proposed telecentric lens versus (a) different deviation distances on the focal plane and (b) different deviation angles at incident angles of 0°, 30°, 55°, and 60°.

This is defined mathematically as a normalized overlap integral between the fiber and wavefront amplitude:

$$T = \frac{\left|\iint F_r(x,y)W^*(x,y)\mathrm{d}x\mathrm{d}y\right|^2}{\iint F_r(x,y)F_r^*(x,y)\mathrm{d}x\mathrm{d}y \iint W(x,y)W^*(x,y)\mathrm{d}x\mathrm{d}y} \tag{2}$$

where $F_r(x,y)$ is the function describing the receiving fiber complex amplitude, $W(x,y)$ is the function describing the complex amplitude of the wavefront from the exit pupil of the optical system, and $(\cdot)^*$ represents the complex conjugate operation. Note that these functions are complex-valued, so this is a coherent overlap integral. T has a maximum possible value of 1.0 and will decrease if there is any mismatch between the fiber amplitude and phase and the wavefront amplitude and phase.

The total power coupling efficiency is the product of S and T. A theoretical maximum coupling efficiency can be computed, and this value is based upon ignoring the aberrations but accounting for all vignetting, transmission, and other amplitude mismatches between the modes.

B. The Evaluation of the Telecentric Lens

Fig. 1(f) presents the simulation configuration, ray tracing, and spot diagrams at angles of 0°, 30°, 55°, and 60° for incident beams. Most spots in spot diagrams at each angle are distributed within the Airy disk, indicating the good focusing capacity, although minor coma exists at large incident angles. Clearly, the chief ray of incident beams is parallel to the axis of the lens in the image space, so that both incident and retro-reflected beams share the same propagation path. Besides, the NA of the lens is almost equal to the one of SMF, ensuring high coupling efficiency for co-propagation.

We further simulate the coupling tolerance of the MRR system when building up the LoS link. In the simulation, we first find the optimum lateral position of the fiber end-face on the focal plane for couping at incident angles of 0°, 30°, 55°, and 60°. Then, the impacts of the deviation of lateral distance and incident angles are evaluated respectively. Fig. 2(a) shows that, for deviation of the lateral distance, angles with high coupling efficiency in the optimum position (0 μm) show a larger tolerance than angles with low coupling efficiency. And the tolerance of coupling efficiency reduced by 3 dB is beyond 5 μm. The evaluation for the effect of the deviation angle is presented in Fig. 2(b), we can see that the tolerance for wide angles is better than the narrow angles, which is beyond 0.05° when coupling efficiency drops by 3 dB. Although these results are somewhat rigorous, for further deployment, a stabilizer with a closed feedback loop can be used to mitigate or eliminate the influence.

III. Experimental Setup

Fig. 3(a) shows the schematic of the bidirectional FSO system using image space telecentric lens-based MRR. The light source is provided by a continuous-wave (CW) laser with optical power of 13.33 dBm at 1550 nm. For downlink communication, it is modulated by 10-Gbit/s OOK sequence generated by a pseudo-random binary sequence (PRBS) generator via a MZM (MZM1) at the transmitter. The modulated optical signals are then amplified by means of an erbium-doped-fiber amplifier (EDFA1) and launched into free space through a fiber collimator used for beam narrowing with optical power of 17.72 dBm at point O. Note that as a proof-of-concept experimental demonstration of the feasibility and effectiveness of the designed telecentric lens-based MRR system, a free-space transmission distance of 3 m is conducted in this article. It can be envisioned that by increasing the power of the transmitter, the MRR-based FSO system with a longer transmission distance can be realized. After 3-m transmission, incident beam impinges on the Rx optics at an angle of θ. Then the downstream signal is coupled into an optical fiber positioned at the focal plane. Due to the limited length of the optical table, the transmission distance is prolonged to 3 m by two high-reflectivity mirrors (M1 and M2) in our experiment (Fig. 3(b)). Also, Rx optics (Fig. 3(c)) is positioned at the center of a rotatable platform. In the experiment, we fix the transceiver

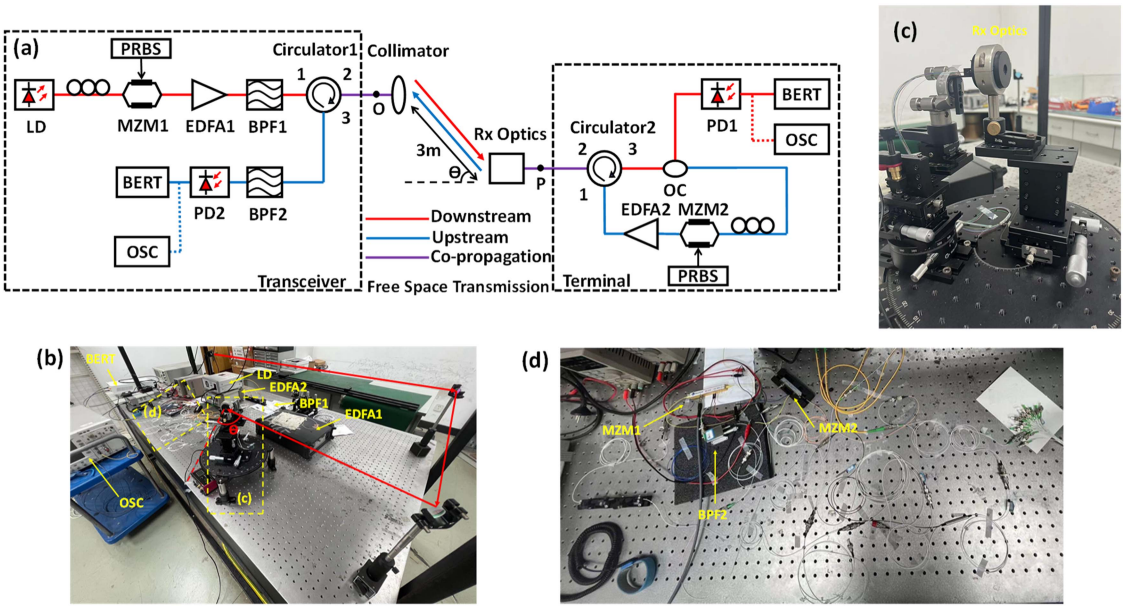

Fig. 3. (a) The schematic of the bidirectional FSO system using image space telecentric lens as Rx optics; (b)–(d) The experimental setup figure of the FSO system. LD: laser diode; PRBS: pseudo-random binary sequence; MZM: Mach-Zehnder modulator; EDFA: erbium-doped-fiber amplifier; BPF: bandpass filter; OC: optical coupler; PD: photodetector; BERT: bit error rate tester; OSC: oscilloscope.

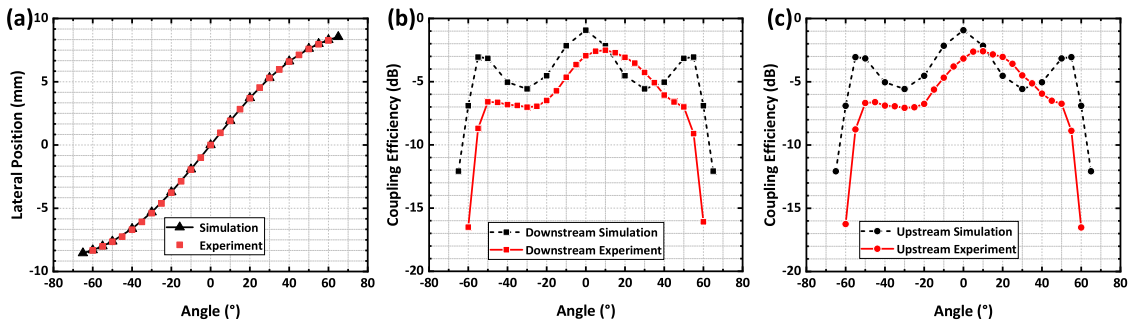

Fig. 4. (a) The lateral position of focal points for different incident angles on the focal plane; the coupling efficiency of the proposed MRR versus different angles for (b) the simulated and measured downstream signal and (c) the simulated and measured upstream signal.

part while rotating the whole Rx optics to simulate different incident angles θ.

At the terminal, the downstream OOK signal is equally split into two branches. One branch is sent into a photodetector (PD1), where the eye diagram is observed using an oscilloscope (OSC) and the BER is measured using a BER tester (BERT). The other branch of the downstream optical signal is sent into another MZM (MZM2) and modulated by a 10-Gbit/s or 5-Gbit/s OOK sequence as the upstream signals. The upstream OOK signal is then amplified to 10 dBm by EDFA2 and launched into free space through circulator2 and Rx optics. The retro-reflected optical signal (upstream OOK optical signal) transmits back to the transceiver through the same free-space optical propagation path and is received by another PD (PD2) through circulator1. The eye diagram and BER of the upstream signals are also measured. Two bandpass filters (BPFs) are placed after EDFA1 and EDFA2 to reduce the noise. The experimental details of the setup are shown in Fig. 3(b)–(d).

IV. Experimental Results and Discussion

A. Coupling Loss

To experimentally measure the coupling loss of both downstream and upstream signals at different incident angles, we place a light source at point O(P), and the optical power is measured at point P(O) (see Fig. 3(a)). The coupling loss is defined as the ratio of power at point P(O) to point O(P). The downstream signals at each angle incident on the corresponding lateral positions on the focal plane are also measured. As is shown in Fig. 4(a), the simulation and experiment share identical results of the lateral distance of these spots, which are within 16 mm between $-60°$ and $+60°$. This good coincidence also suggests that a customized fiber array may be used to collect signals from different incident angles in this large FOV.

Fig. 4(b) shows the simulated and measured coupling loss of the downstream signals. The simulated coupling loss is down to 5.6 dB between $-50°$ and $+50°$, 6.9 dB between $-60°$

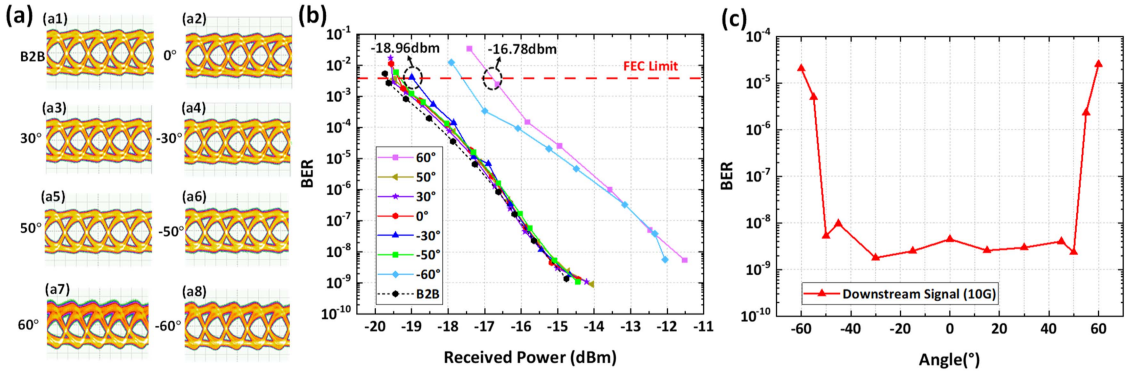

Fig. 5. (a) Eye diagrams of the 10-Gbit/s downstream signals in B2B link and at different incident angles (50 ps/div); (b) BER results of 10-Gbit/s downstream signals as received optical power varies; (c) BER results of 10-Gbit/s downstream signals as incident angle varies with a received optical power of −15 dBm.

and +60°, and 12.1 dB between −65° and +65°, while the measured coupling loss is down to 7 dB between −50° and +50°, 8.9 dB between −55° and +55, and 16.5 dB between −60° and +60°, slightly larger than the simulated results. The coupling loss of the upstream signals is depicted in Fig. 4(c), which is comparatively the same as downstream signals shown in Fig. 4(b), and beyond 110°, the energy attenuation soars for both cases. For simulated results, the efficiency at positive and negative angles are identical, while for experimental results, the maximum coupling efficiency occurs at around 10° where the coupling loss is about 2.6 dB. In general, the experimental results and simulation results fit well. The deviation could result from the assembly error during lens fabrication, misalignment between the incident beam and the pupil of Rx optics, the divergence of the beam caused by the adjustment error of the collimator, and distortion of the wavefront after two reflections.

B. Downstream Performance

Fig. 5(a2)–(a8) present the measured eye diagrams of the 10-Gbit/s downstream signals at different incident angles. One can see that the eye-opening is almost the same between +50° and −50°. And little jitters are introduced at +60° and −60°. As a comparison, direct communication results through the optical fiber back-to-back (B2B) rather than free space transmission are presented in Fig. 5(a1). In general, the noise introduced by free space is extremely low and signals show high quality.

The BER performance of the downstream optical signal transmitting at different incident angles and the B2B results for comparison are shown in Fig. 5(b), where the least required received powers for the incident angles of the downstream signal between +60° and −60°, between +50° and −50°, and B2B are −16.78 dBm, −18.96 dBm, −19.69 dBm respectively, at the 7%-overhead hard-decision forward error correction (HD-FEC) limit of BER @3.8 × 10^{-3}. Also, between +50° and −50°, the same performance for each angle is achieved in the system, similar to the B2B performance. The BER performance at +60° and −60° slightly declined as compared to angles between +50° and −50°. We also show the BER of the downstream optical signals at a data rate of 10 Gbit/s at different incident angles with a fixed received optical power of −15 dBm. As is shown in Fig. 5(c), for angles between +60° and −60°, the BERs of the downstream signals measured are all below 1 × 10^{-4}. Between 50° and −50°, the BER performances are almost the same and are below 1 × 10^{-8}. Outside 50° and −50°, the BER performance deteriorates rapidly. The decline of BER performance could be attributed to the dramatical increase of the coupling loss at large angles around +60° and −60° and the intensified distortion of the optical wavefront as the angle increases.

C. Upstream Performance

Next, we explore the uplink performance of the proposed MRR system. Fig. 6(a1)–(a6) present the eye diagrams of the 10-Gbit/s upstream signals at different incident angles and B2B result for comparison; Fig. 6(a7)–(a12) show the eye diagrams of the 5-Gbit/s upstream signals. It is seen that at each data rate, the eye openings of the free-space link decrease as compared to B2B link due to the noises introduced in the optical paths such as the reflected lights from the fiber end-face. Also, at each data rate, the quality of the eye diagram at positive angles is better than that at negative angles, which owes to that the reflected light from the fiber end-face is more intense than that at positive angles, deteriorating the signal-to-noise ratio (SNR) of the retro-reflected signal.

Fig. 6(b) shows the BER performance of the upstream optical signals at a data rate of 10 Gbit/s at different incident angles, and the B2B link is also provided as a reference. We can see that the least required received powers for the upstream signal for angles between +50° and −50°, and B2B are −7.80 dBm and −17.97 dBm respectively at the BER of 3.8 × 10^{-3}. Fig. 6(c) shows the BER performance of the upstream optical signals at a data rate of 5 Gbit/s at different incident angles. It is observed that the least required received powers for the upstream signals at angles between +50° and −50°, and B2B are −15.97 dBm and −22.21 dBm respectively at the BER of 3.8 × 10^{-3}. The BERs of upstream optical signals at data rates of 10 Gbit/s and 5 Gbit/s are also measured with a received optical power of −5 dBm as incident angle varies. As is shown in Fig. 7, for angles between +55° and −55°, the BERs of the upstream signals at a data rate of both 10 Gbit/s and 5 Gbit/s measured are below the HD-FEC

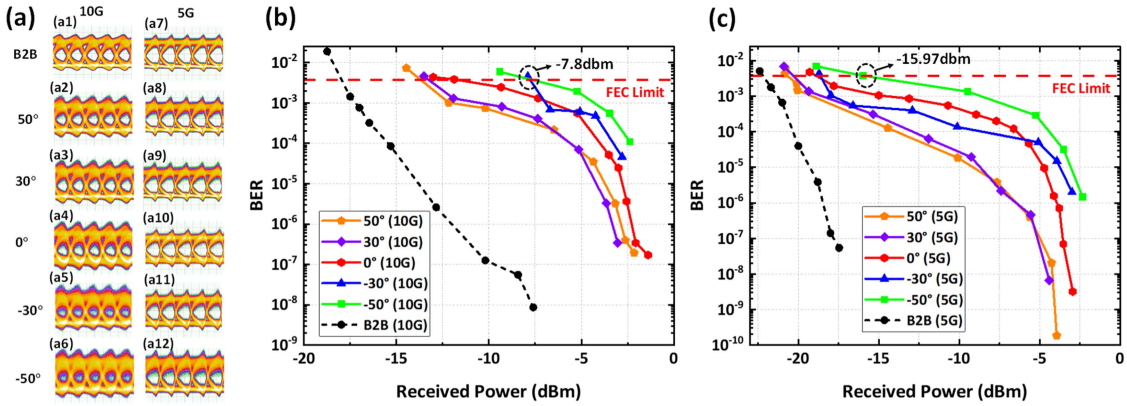

Fig. 6. (a) Eye diagrams of the 10-Gbit/s upstream signals (50 ps/div) and 5-Gbit/s upstream signals (100 ps/div) in B2B link and at different incident angles; (b) BER results of 10-Gbit/s upstream signals as received optical power varies; (c) BER results of 5-Gbit/s upstream signals as received optical power varies.

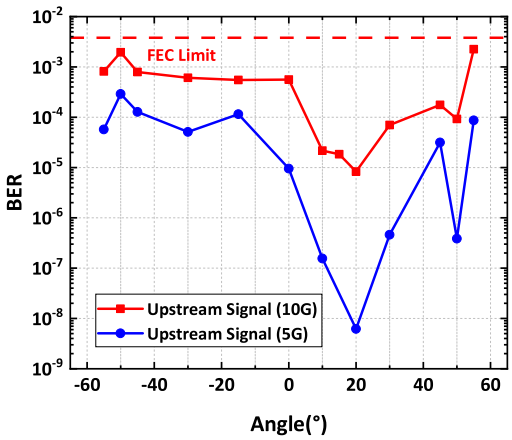

Fig. 7. BER results of upstream signals as incident angle varies with a received optical power of −5 dBm.

BER limit, manifesting a wide-FOV of up to 110° for our MRR system. Obviously, the BER performance at a data rate of 5 Gbit/s is better than that at a data rate of 10 Gbit/s. As can be seen from Figs. 6(b), (c), and 7, same as eye diagrams in Fig. 6(a1)–(a6) and Fig. 6(a7)–(a12), the BER performance at the positive angles is generally better than the negative angles. And when the incident angle becomes larger, the BER performance decreases. A better performance occurs at the angles of 30° and 50° rather than 0°. This can be explained as follows. A large amount of light would reflect from the fiber end-face at normal incident angles. This reflected light can strongly disturb the upstream optical signals and decrease the SNR of the upstream signals. Therefore, even with a lower coupling loss than 0°, a better SNR happens at larger incident angles. In this case, the measurement could be taken by tilting the fiber end-face a few degrees though sacrificing the coupling ratio to some extent. In short, a more delicate balance between the coupling ratio and reflected power needs to be manipulated for a higher SNR.

V. Discussion

For practical applications, one approach to automatically couple the beam into the MRR system could be the utilization of ATP systems integrated in the transceiver. These systems would enable the measurement of both the distance between the transceiver and terminal, and the incident angle of beams [27]. The information collected from these measurements can be transmitted to the terminal through traditional RF communication. In the terminal, it could precisely calculate the position of the focal point on the focal plane according to the information acquired from the transceiver (see Fig. 4(a)) and move the fiber to the calculated position employing a motorized linear stage.

Additionally, to facilitate the demonstration, OOK signals are employed for both downlink and uplink in our half-duplex FSO system. However, duplex high-speed communications could also be achieved in our proposed MRR system by means of adopting two different modulation methods that can be operated simultaneously in bidirectional communications like differential phase shift keying (DPSK) signals used in downlink and OOK signals used in uplink [26]. Also, to further increase the transmission speed and system capacity, employing advanced modulation formats like quadrature phase-shift keying (QPSK) signals [28] and multiple-dimensional multiplexing of orbital angular momentum [29], [30], polarization, and wavelength [31], [32] can be considered. Furthermore, lower required received optical powers are able to be obtained by integrating an optical amplifier with a photodetector, which enables larger FOV, longer transmission distance, and higher tolerance for misalignment.

Note that an EDFA amplifier is adopted at the terminal in our experiment. This is a tradeoff for a better SNR. To achieve a true MRR system with only one light source, one needs to increase the power of the incident light and coupling efficiency to compensate for the insertion loss for numerous devices like modulators, splitters, and circulators. In addition, reducing the noise caused by various optical components in the system to increase the SNR of the retro-reflected signal, like depositing the fiber end-face with infrared anti-reflective coating, must be considered.

In the future, more experiments based on our proposed MRR system in longer transmission distances could be conducted, allowing for a more comprehensive analysis of the communication system's performance, as well as a detailed study of the potential

factors that might influence it. Concurrently, some measures could be implemented to handle the disturbance introduced by the atmosphere, like beam focusing and directional techniques, adaptive optics, and increasing the gain of optical amplifiers. And our wide-FOV and high-speed MRR system carries the potential to provide an efficient and viable way for a variety of specific aspects, like swift FSO network transmission and deployment, military applications, cloud computing, and big data processing. Furthermore, the ongoing advancements in integration technology could catalyze the realization of more miniaturized and cost-effective MRR, thus fostering its broader implementation.

VI. Conclusion

In order to alleviate the difficulty of precisely establishing a narrow LoS between the transceiver and terminal, thus leading to the further application of the FSO communication technology to medium and small platforms (e.g., aircraft and satellites), a novel wide-FOV MRR using an image space telecentric lens has been proposed and a bidirectional FSO communication system has been experimentally demonstrated with a single light source. The performance of the MRR has been assessed by both simulation and experiment, showing a low coupling loss less than 9.1 dB within 110°. The bidirectional FSO transmission performance based on the MRR has been evaluated by observing eye diagrams and measuring BER results of both 10-Gbit/s OOK downstream and 10-Gbit/s (5-Gbit/s) OOK upstream signals at different incident angles. The transmission bit rate and SNR are expected to be improved by decreasing both the coupling loss of the lens and the end-face reflection of all components in the system. The proposed MRR system has a wide-FOV of up to 110°, which is the largest compared to all reported works for FSO communications.

References

[1] T. Koonen, "Indoor optical wireless systems: Technology, trends, and applications," *J. Lightw. Technol.*, vol. 36, no. 8, pp. 1459–1467, Apr. 2018.

[2] M. Z. Chowdhury, M. T. Hossan, A. Islam, and Y. M. Jang, "A comparative survey of optical wireless technologies: Architectures and applications," *IEEE Access*, vol. 6, pp. 9819–9840, 2018.

[3] M. A. Khalighi and M. Uysal, "Survey on free space optical communication: A communication theory perspective," *IEEE Commun. Surveys Tuts.*, vol. 16, no. 4, pp. 2231–2258, Fourthquarter 2014.

[4] S. A. Al-Gailani et al., "A survey of free space optics (FSO) communication systems, links, and networks," *IEEE Access*, vol. 9, pp. 7353–7373, 2021.

[5] A. Jahid, M. H. Alsharif, and T. J. Hall, "A contemporary survey on free space optical communication: Potentials, technical challenges, recent advances and research direction," *J. Netw. Comput. Appl.*, vol. 200, Apr. 2022, Art. no. 103311.

[6] C. Fei et al., "100-m/3-gbps underwater wireless optical transmission using a wideband photomultiplier tube (PMT)," *Opt. Exp.*, vol. 30, no. 2, pp. 2326–2337, 2022.

[7] O. Aboelala, I. E. Lee, and G. C. Chung, "A survey of hybrid free space optics (FSO) communication networks to achieve 5G connectivity for backhauling," *Entropy*, vol. 24, no. 11, Oct. 2022, Art. no. 1573.

[8] K. Wang, A. Nirmalathas, C. Lim, K. Alameh, and E. Skafidas, "Fullduplex gigabit indoor optical wireless communication system with CAP modulation," *IEEE Photon. Technol. Lett.*, vol. 28, no. 7, pp. 790–793, Apr. 2016.

[9] Y. Hong et al., "Demonstration of >1Tbit/s WDM OWC with wavelength-transparent beam tracking-and-steering capability," *Opt. Exp.*, vol. 29, no. 21, pp. 33694–33702, 2021.

[10] R. Abdelfatah, N. Alshaer, and T. Ismail, "A review on pointing, acquisition, and tracking approaches in UAV-based FSO communication systems," *Opt. Quantum Electron.*, vol. 54, no. 9, pp. 1–16, Jul. 2022.

[11] G. G. Peter et al., "Modulating retro-reflector lasercom systems at the Naval Research Laboratory," in *Proc. IEEE Mil. Commun. Conf.*, 2010, pp. 1601–1606.

[12] G. C. Gilbreath et al., "Large-aperture multiple quantum well modulating retroreflector for free-space optical data transfer on unmanned aerial vehicles," *Opt. Eng.*, vol. 40, no. 7, pp. 1348–1356, Jul. 2001.

[13] N. Saeed, H. Almorad, H. Dahrouj, T. Y. Al-Naffouri, J. S. Shamma, and M.-S. Alouini, "Point-to-point communication in integrated satellite-aerial 6G networks: State-of-the-Art and future challenges," *IEEE Open J. Commun. Soc.*, vol. 2, pp. 1505–1525, 2021.

[14] C. Quintana et al., "A high speed retro-reflective free space optics links with UAV," *J. Lightw. Technol.*, vol. 39, no. 18, pp. 5699–5705, Sep. 2021.

[15] M. T. Dabiri et al., "Modulating retroreflector based free space optical link for UAV-to-ground communications," *IEEE Trans. Wireless Commun.*, vol. 21, no. 10, pp. 8631–8645, Oct. 2022.

[16] C. M. Swenson, C. A. Steed, I. A. D. L. Rue, and R. Q. Fugate, "Low-power FLC-based retromodulator communications system," *Proc. SPIE*, vol. 2990, pp. 296–310, Apr. 1997.

[17] R. Mahon et al., "Underwater optical modulating retro-reflector links," in *Proc. Appl. Lasers Sens. Free Space Commun.*, 2010, Paper LSTuB1.

[18] Y. Chen, Y. Wang, and J. Tsai, "Study of wire electrical discharge machined folded-up corner cube retroreflector with a tunable cantilever beam," *Opt. Eng.*, vol. 57, no. 3, Mar. 2018, Art. no. 035104.

[19] G. Yang et al., "Wavefront compensation with the micro corner-cube reflector array in modulating retroreflector free-space optical channels," *J. Lightw. Technol.*, vol. 39, no. 5, pp. 1355–1363, Mar. 2021.

[20] W. S. Rabinovich et al., "A cat's eye multiple quantum-well modulating retro-reflector," *IEEE Photon. Technol. Lett.*, vol. 15, no. 3, pp. 461–463, Mar. 2003.

[21] J. Öhgren et al., "A high-speed modulated retro-reflector communication link with a transmissive modulator in a cat's eye optics arrangement," *Proc. SPIE*, vol. 6736, 2007, Art. no. 673619.

[22] Y. Fan, L. Zhang, B. Liu, F. Chu, and S. Fang, "The influence of cat's eye effect on CEMRR FSO gain under defocus oblique incidence," *Proc. SPIE*, vol. 11562, 2020, Art. no. 115620M.

[23] G. Spirou et al., "A high-speed modulated retro-reflector for lasers," in *Proc. IEEE Aerosp. Conf.*, 2002, p. 3.

[24] C. Quintana et al., "High speed electro-absorption modulator for long range retroreflective free space optics," *IEEE Photon. Technol. Lett.*, vol. 29, no. 9, pp. 707–710, May 2017.

[25] T. M. Shay and R. Kumar, "2.5-Gbps amplified retromodulator for free-space optical communications," *Proc. SPIE*, vol. 5550, pp. 122–129, Oct. 2004.

[26] X. Wang, X. Feng, P. Zhang, T. Wang, and S. Gao, "Single-source bidirectional free-space optical communications using reflective SOA-based amplified modulating retro-reflection," *Opt. Commun.*, vol. 387, pp. 43–47, 2017.

[27] Z. Li et al., "LiDAR integrated IR OWC system with the abilities of user localization and high-speed data transmission," *Opt. Exp.*, vol. 30, no. 12, pp. 20796–20808, Jun. 2022.

[28] X. Feng, H. Jiang, Z. Wu, T. Wang, H. Jiang, and S. Gao, "60 Gbit/s coherent wavelength-division multiplexing free-space optical modulating retro-reflector in a turbulence-tunable atmospheric cell," *Opt. Commun.*, vol. 448, pp. 111–115, 2019.

[29] J. Wang et al., "Terabit free-space data transmission employing orbital angular momentum multiplexing," *Nature Photon.*, vol. 6, no. 7, pp. 488–496, Jun. 2012.

[30] J. Wang, J. Liu, S. Li, Y. Zhao, J. Du, and L. Zhu, "Orbital angular momentum and beyond in free-space optical communications," *Nanophotonics*, vol. 11, no. 4, pp. 645–680, 2022.

[31] H. Huang et al., "100 Tbit/s free-space data link enabled by three-dimensional multiplexing of orbital angular momentum, polarization, and wavelength," *Opt. Lett.*, vol. 39, no. 2, pp. 197–200, 2014.

[32] S. N. Khonina, N. L. Kazanskiy, M. A. Butt, and S. V. Karpeev, "Optical multiplexing techniques and their marriage for on-chip and optical fiber communication: A review," *Opto-Electron. Adv.*, vol. 5, no. 8, 2022, Art. no. 210127.